Supplement of Hydrol. Earth Syst. Sci., 30, 2357–2372, 2026
https://doi.org/10.5194/hess-30-2357-2026-supplement

Hydrology and Earth System Sciences
Open Access
EGU

Supplement of

Seasonal dynamics of closed shallow lakes nutrient status controlled by lacustrine groundwater discharge

Xiaoliang Sun et al.

Correspondence to: Yao Du (yaodu@cug.edu.cn)

S1. ^{222}Rn mass balance model

In recent years, ^{222}Rn has been extensively applied in LGD studies (Adyasari et al., 2023). Originating from its predecessor, ^{226}Ra, ^{222}Rn has a half-life of 3.82 d. By treating lake water as a defined system, a mass balance model was established based on both its sources and sinks of ^{222}Rn. The ^{222}Rn flux of groundwater discharge was deduced as an unidentified term. The ^{222}Rn mass balance model structure can be expressed as follows (Kluge et al., 2007; Schmidt et al., 2010; Luo et al., 2018; Dabrowski et al., 2020; Sun et al., 2024):

$$\frac{\partial I^{222}Rn}{\partial t} = F_g + F_d + I^{226}Ra \times \lambda^{222}Rn - F_a - I^{222}Rn \times \lambda^{222}Rn \quad \text{(S1)}$$

where F_g, F_d, and F_a are the ^{222}Rn flux (Bq/m^{2}d) of groundwater discharge, sediment diffusion, and atmospheric escape, respectively. I^{226}Ra and I^{222}Rn are the pools of ^{226}Ra and ^{222}Rn in the lake water (Bq/m^2), which are equal to the concentrations of ^{226}Ra and ^{222}Rn multiplied by the water depth. The λ^{222}Rn is the decay coefficient of ^{222}Rn with a value of 0.181 d^{-1}. During the field sampling period at each lake, we selected two identical sites in the lake to measure the ^{222}Rn concentration and lake water level before and after sampling. This was done to compare the changes in ^{222}Rn concentration and water level before and after sampling. The measurement times before and after sampling were the first day and the last day of the sampling period, respectively. Since there is almost no difference in the lake water level and ^{222}Rn concentration at the same location before and after sampling, the change in the ^{222}Rn in lake water on the left side of the equation can be approximated as 0 (Kluge et al., 2007; Dimova et al. 2013; Liao et al., 2022).

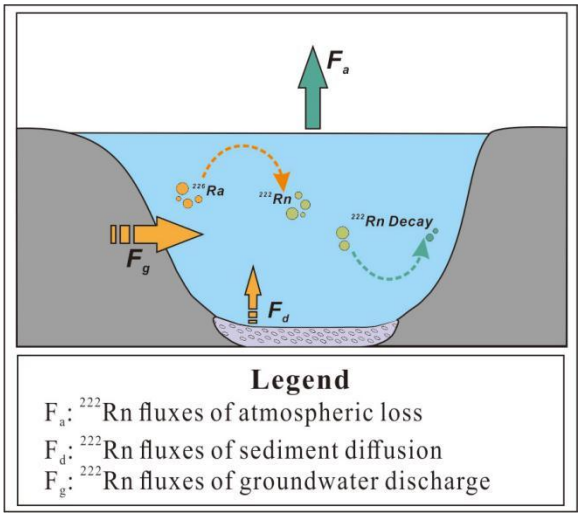

Figure S1. Conceptual diagram of source and sink terms in the lake ^{222}Rn mass balance model.

Figure S1. Conceptual diagram of source and sink terms in the lake ^{222}Rn mass balance model.

The ^{222}Rn flux diffused from the sediment to the lake is one source of the ^{222}Rn mass balance model, and it is calculated by the following formula (Wang et al., 2020):

$$F_d = \sqrt{\left(\lambda^{222}Rn \times nD_m\right)}\left(C_{\mathrm{p}} - C_w\right) \tag{S2}$$

where C_p (Bq/m^3) and C_w (Bq/m^3) are ^{222}Rn concentrations of pore water in sediments and overlying lake water, respectively; D_m (cm^2/s) is the ^{222}Rn molecular diffusion coefficient in wet bulk sediment (Boudreau, 1996; Cable et al., 1996; Schulz, 2006), n is the porosity of the sediment.

To determine the ^{222}Rn concentrations in sediment pore water, a sediment equilibrium incubation experiment was carried out following the procedure proposed by Corbett et al. (1998). The D_m is expressed as:

$$-\log \mathrm{D_m} = \left(\frac{980}{T_{\mathrm{w}} + 273}\right) + 1.59 \tag{S3}$$

where T_w is water temperature (°C). An equilibrium incubation experiment with lakebed sediments was carried out to obtain the ^{222}Rn concentration in sediment pore water (Corbett et al., 1998). 150 g of sediment and 500 mL of in-situ lake water were placed in an Erlenmeyer flask and sealed. The lake bed sediment and overlying lake water were incubated in a shaker for 30 days until the ^{222}Rn concentration in sediment pore water reached equilibrium. The balanced lake water was transferred to 250 mL glass bottles by overflow method and then measured with RAD7 and RAD H_2O.

The ^{222}Rn concentration in lake water is higher than that in air. As a result, ^{222}Rn in lake water will escape from the water-gas interface to the atmosphere under the effect of the ^{222}Rn concentration gradient between them. The atmospheric loss of ^{222}Rn is estimated based on the following empirical equation, which is related to temperature and wind speed (MacIntyre et al., 1995; Schmidt and Schubert, 2007; Dimova and Burnett, 2011):

$$F_{\mathrm{a}} = K\left(C_w - \alpha C_a\right) \tag{S4}$$

$$\partial = 0.105 + 0.405\ \mathrm{e}^{-0.0502\ Tw} \tag{S5}$$

$$K = 0.45\ \mu_{10}^{1.6} \times \left(\frac{S_C}{600}\right)^{-\mathrm{b}} \tag{S6}$$

$$\mu_{10} = \mu_h \left[0.097 \ln(\frac{h}{10}) + 1 \right]^{-1} \quad \text{(S7)}$$

where K values are in cm h^{-1} but have been scaled to m d^{-1} for input into Eq. (6); C_w is the concentration of lake water ^{222}Rn (Bq/m^3); C_a is the concentration of ^{222}Rn in the air (Bq/m^3); α is the gas distribution coefficient (dimensionless) and is a temperature dependent function (Burnett and Dulaiova, 2003); T_w (°C) was the temperature of the lake water; b = 0.5 when wind speed > 3.6 m/s and b = 0.667 when wind speed < 3.6 m/s; μ_{10} is the wind speed (m/s) at 10 m above lake surface; μ_h is the wind speed at measurement height (m/s), h is the wind observation elevation (m) above the lake water surface, wind speed (m/s) data during the study period were average 15 minutes wind speed obtained from portable weather station monitored in lake area; Sc (dimensionless) is the influence of kinematic viscosity (v) and the molecular diffusion coefficient (D_m), and can be expressed as:

$$S_C = \frac{v}{D_m} = \frac{\eta}{\rho D_m} \quad \text{(S8)}$$

where v (m^2/s) is the kinematic viscosity which equals the ratio of absolute viscosity (η) [kg/(m d)] to water density (ρ) (kg/m^3) at specific temperature Dm and v are related to temperature changes.

$$\eta = A \times 10^{B/(Tw-C)} \quad \text{(S9)}$$

where constants A, B and C are 2.414×10^{-5} kg/(m s), 247.8 K and 140 K, respectively.

Generally, ^{222}Rn from the decay of dissolved ^{226}Ra can be omitted for ^{222}Rn mass balance model (Yi et al., 2018). Radium is generally adsorbed onto the surface of particle in fresh water (Wang et al., 2021) and is only released from the surface of particles into water in brackish or salt water environments (Webster et al., 1995, Gonneea et al., 2008). In freshwater lake environments, the concentration of ^{226}Ra is very low as to be negligible (Dimova et al., 2013; Luo et al., 2018). To verify this point of view, a simple experiment was conducted in which two lake water samples were degassed and then sealed (Corbett et al., 1997; Dimova et al., 2015). After 28 days, ^{222}Rn was not detected in both lake water samples, indicating that ^{226}Ra would not significantly contribute to ^{222}Rn in lake water.

The LGD rate can be obtained by dividing the ^{222}Rn flux from groundwater discharge by the ^{222}Rn concentration of surrounding groundwater. The formula is as follows (Luo et al., 2018; Wang et al., 2019):

$$V = \frac{F_g}{C_g} \times 1000 \quad \text{(S10)}$$

where V is the average LGD rate (mm/d); Fg is the ^{222}Rn flux of groundwater discharge [Bq/(m^2 d)]; Cg is the ^{222}Rn concentrations in groundwater end member (Bq/m^3).

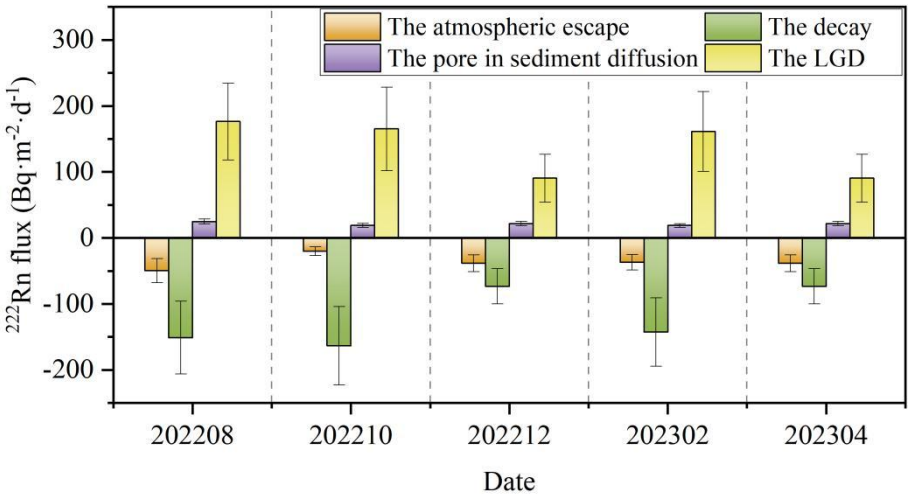

Figure S2. The ^{222}Rn source and sink fluxes in different periods.

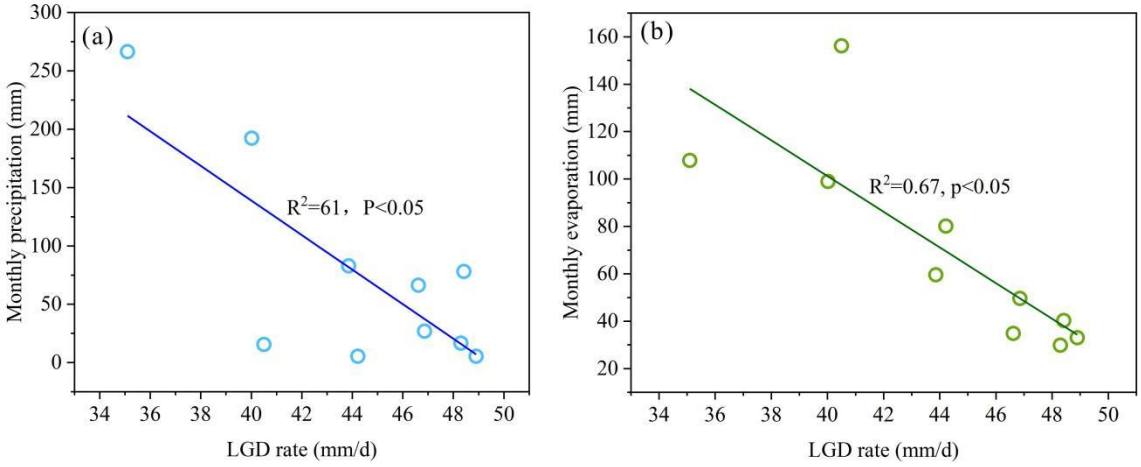

Figure S3. The correlation between the simulated LGD rate and monthly precipitation and monthly evaporation volume.

Table S1. The fluxes of nutrients from sediment diffusion and atmospheric deposition for individual sampling sites.

Sampling site	Diffusive fluxes from the sediment to the overlying water ($mg/m^2/d$)			Atmospheric total deposition fluxes ($mg/m^2/d$)		
	NH_4-N	TN	TP	NH_4-N	TN	TP
HWL02	0.39	2.46	0.005	0.46	1.26	0.02
HWL03	0.67	0.45	0.005	0.46	1.39	0.03
HWL06	0.34	0.32	0.003	0.50	1.27	0.03

Table S2. The average fluxes of nutrients from sediment diffusion and atmospheric deposition for HWL.

Lake	Diffusive fluxes from the sediment to the overlying water ($mg/m^2/d$)			Atmospheric total deposition fluxes ($mg/m^2/d$)		
	NH_4-N	TN	TP	NH_4-N	TN	TP
HWL	0.47	1.08	0.004	0.47	1.31	0.03

S2. Mechanistic analysis of changes in groundwater TP concentration

To investigate the mechanisms driving TP concentration dynamics, we further examined key hydrogeochemical parameters, including electrical conductivity (EC), dissolved oxygen (DO), and redox potential (Eh) (Table S3). Based on monitoring data from August 2022 to April 2023, the TP dynamics can be roughly divided into three stages:

(1) Aug–Dec 2022 (TP rise followed by decline): During this period, Eh increased markedly from −97.43 mV to −56.24 mV, and DO rose from 1.24 to 2.60 $mg \cdot L^{-1}$, indicating rapid aquifer oxidation. In the early oxidation phase (up to October), "oxidative dissolution" of phosphate-bearing minerals may have temporarily elevated TP to 2.00×10^{-2} $mmol \cdot L^{-1}$. Subsequently, strong oxidative conditions promoted the formation of iron and manganese oxides, which adsorbed phosphorus. Although EC increased from 823.83 to 942.61 $\mu S \cdot cm^{-1}$, suggesting an increase in

competitive anions, adsorption dominated, and TP ultimately declined to the monitoring minimum of 6.46×10^{-3} mmol·L^{-1} by December.

(2) Dec 2022–Feb 2023 (TP increase): Eh continued to rise substantially to −27.26 mV, and DO remained relatively high at 2.29 mg·L^{-1}, indicating that the system had not returned to a reducing state. The TP peak (2.19×10^{-2} mmol·L^{-1}) during this stage was therefore not due to reductive release. Instead, it was primarily driven by external phosphorus inputs associated with enhanced precipitation and agricultural activities. Meanwhile, EC reached the monitoring-period maximum of 973.69 μS·cm^{-1}, indicating the influx of high concentrations of dissolved salts. These competitive anions may have temporarily weakened sediment phosphorus retention, jointly contributing to the TP increase.

(3) Feb–Apr 2023 (TP decline): Oxidative conditions intensified further, with Eh and DO reaching the monitoring-period maximum values of −13.94 mV and 3.58 mg·L^{-1}, respectively. Strong oxidative adsorption dominated once again, effectively removing most of the previously input phosphorus. Despite EC remaining high (961.83 μS·cm^{-1}), TP concentration declined substantially to 8.24×10^{-3} mmol·L^{-1} by April.

Overall, the fluctuations in TP concentration reflect the combined effects of internal adsorption and fixation, external input pulses, and geochemical competition (as indicated by EC changes) under a macro-scale context of aquifer oxidation driven by declining water levels (Eh and DO continuously increasing).

Table S3. EC, DO and Eh values in groundwater for each sampling period.

Date	Groundwater EC (μS·cm^{-1})	Groundwater DO (mg·L^{-1})	Groundwater Eh (mv)
08/2022	823.83	1.24	-97.43
10/2022	920.44	1.41	-81.26
12/2022	942.61	2.6	-56.24
02/2023	973.69	2.29	-27.26
04/2023	961.83	3.58	-13.94

References

Adyasari, D., Dimova, N. T., Dulai, H., Gilfedder, B. S., Cartwright, I., McKenzie, T., & Fuleky, P. (2023). Radon-222 as a groundwater discharge tracer to surface waters. Earth-Science Reviews, 104321.

Boudreau, B.P. (1996). The diffusive tortuosity of fine-grained unlithified sediments. Geochimica et Cosmochimica Acta, 60(16), 3139–3142.

Burnett, W. C., Wattayakorn, G., Supcharoen, R., Sioudom, K., Kum, V., Chanyotha, S., & Kritsananuwat, R. (2017). Groundwater discharge and phosphorus dynamics in a flood-pulse system: Tonle Sap Lake, Cambodia. Journal of Hydrology, 549, 79–91.

Burnett, W.C., & Dulaiova, H. (2003). Estimating the dynamics of groundwater input into the coastal zone via continuous radon-222 measurements. Journal of Environmental Radioactivity, 69(1–2), 21–35.

Cable, J.E., Burnett, W.C., Chanton, J.P., & Weatherly, G. (1996). Modeling groundwater flow into the ocean based on ^{222}Rn. Earth Planetary Science Letters, 144, 591–604.

Corbett, D.R, Burnett, W., Cable, P., & Clark, S. (1998). A multiple approach to the determination of radon fluxes from sediments. Journal of Radioanalytical and Nuclear Chemistry, 236(1–2), 247–253.

Corbett, D.R., Burnett, W.C., Cable, P.H., & Clark, S.B. (1997). Radon tracing of groundwater input into Par Pond, Savannah River site. Journal of Hydrology, 203(1–4), 209–227.

Dabrowski, J. S., Charette, M. A., Mann, P. J., Ludwig, S. M., Natali, S. M., Holmes, R. M., & Henderson, P. B. (2020). Using radon to quantify groundwater discharge and methane fluxes to a shallow, tundra lake on the Yukon-Kuskokwim Delta, Alaska. Biogeochemistry, 148, 69–89.

Dimova, N. T., & Burnett, W. C. (2011). Evaluation of groundwater discharge into small lakes based on the temporal distribution of radon-222. Limnology and Oceanography, 56(2), 486–494.

Dimova, N. T., Burnett, W. C., Chanton, J. P., & Corbett, J. E. (2013). Application of radon-222 to investigate groundwater discharge into small shallow lakes. Journal of Hydrology, 486, 112–122.

Dimova, N., Paytan, A., Kessler, J.D., Sparrow, K., Garcia-Tigreros Kodovska, F., Lecher, A.L., Murray, J., & Tulaczyk, S.M., (2015). Current magnitude and mechanisms of groundwater discharge in the Arctic: case study from Alaska. Environmental Science & Technology, 49(20), 12036–12043.

Gonneea, M.E., Morris, P.J., Dulaiova, H., & Charette, M.A. (2008). New perspectives on radium behavior within a subterranean estuary. Marine Chemistry, 109(3–4), 250–267.

Kluge, T., Ilmberger, J., Von Rohden, C., & Aeschbach-Hertig, W. (2007). Tracing and quantifying groundwater inflow into lakes using a simple method for radon-222 analysis. Hydrology and Earth System Sciences, 11(5), 1621–1631.

Liao, F., Wang, G., Yang, N., Shi, Z., Li, B., & Chen, X. (2022). Groundwater discharge tracing for a large Ice-Covered lake in the Tibetan Plateau: Integrated satellite remote sensing data, chemical components and isotopes (D, 18O, and ^{222}Rn). Journal of Hydrology, 609, 127741.

Luo, X., Kuang, X.X., Jiao, J.J., Liang, S.H., Mao, R., Zhang, X.L., & Li, H.L. (2018), Evaluation of lacustrine groundwater discharge, hydrologic partitioning, and nutrient budgets in a proglacial lake in the Qinghai-Tibet Plateau: using ^{222}Rn and stable isotopes. Hydrology and Earth System Sciences, 22, 5579–5598.

MacIntyre, S., Wanninkof, R., & Chanton, J.P. (1995). Trace gas exchange across the air-water interface in freshwater and coastal marine environments, in, edited by: Matson, PA and Harriss, RC, Biogenic trace gases: Measuring emissions from soil and water. Methods in Ecology, 52–97.

Schmidt, A., & Schubert, M. (2007). Using radon-222 for tracing groundwater discharge into an open-pit lignite mining lake–a case study. Isotopes in Environmental and Health Studies, 43(4), 387–400.

Schmidt, A., Gibson, J.J., Santos, I.R., Schubert, M., Tattrie, K., & Weiss, H. (2010). The contribution of groundwater discharge to the overall water budget of two typical Boreal lakes in Alberta/Canada estimated from a radon mass balance. Hydrology and Earth System Sciences, 14(1), 79–89.

Sun, X., Du, Y., Wu, J., Xu, J., Tian, H., Deng, Y., & Wang, Y. (2024). Two-decadal variability of lacustrine groundwater discharge: Coupled controls from weather and hydrologic changes. Water Resources Research, 60(10), e2024WR037173.

Sun, X., Du, Y., Xu, J., Tian, H., Deng, Y., Gan, Y., & Wang, Y. (2025). Control of groundwater-lake interaction zone structure on spatial variability of lacustrine groundwater discharge in oxbow lake. Water Resources Research, 61(1), e2024WR039334.

Wang, Q., Li, H., Zhang, Y., Wang, X., Xiao, K., Zhang, X., & Dan, S. F. (2020). Submarine groundwater discharge and its implication for nutrient budgets in the western Bohai Bay, China. Journal of environmental radioactivity, 212, 106132.

Wang, Q., Li, H., Zhang, Y., Wang, X., Zhang, C., Xiao, K., & Qu, W. (2019). Evaluations of submarine groundwater discharge and associated heavy metal fluxes in Bohai Bay, China. Science of the total environment, 695, 133873.

Wang, Q., Zhang, X., Wang, X., Xiao, K., Zhang, Y., Wang, L. et al. (2021). Quantification of the water age and submarine groundwater discharge in a typical semi-enclosed bay using stable oxygen (^{18}O) and radioactive radium (^{228}Ra) isotopes. Journal of Hydrology, 603, 127088.

Webster, I.T., Hancock, G.J., & Murray, A.S. (1995). Modelling the effect of salinity on radium desorption from sediments. Geochimica et Cosmochimica Acta, 59(12), 2469–2476.

Yi, P., Luo, H., Chen, L., Yu, Z.B., Jin, H.J., Chen, X.B., et al. (2018). Evaluation of groundwater discharge into surface water by using radon-222 in the source area of the yellow river, qinghai-tibet plateau, Journal of Environmental Radioactivity, 192, 257.